$K_{18}Tl_{20}Au_3$: A Novel Derivative of K_8Tl_{11} with the Unprecedented Polyanion $Tl_9Au_2^{9-}$, the Parent Tl_{11}^{7-}, and an Isolated Au^- Ion

Zhen-Chao Dong and John D. Corbett*

Ames Laboratory—DOE[1] and Department of Chemistry, Iowa State University, Ames, Iowa 50011

Received March 8, 1995[⊗]

Attempts to derivatize the novel Tl_{11}^{7-} ions in K_8Tl_{11} by Au substitution leads to the formation of the title compound from direct reaction of the elements in Ta tubing at 500 and then 350 °C. The crystal structure was established at room temperature by single crystal X-ray diffraction means (space group $P\bar{6}m2$, $Z = 1$, $a = 10.880$ (1), $c = 14.552$ (2) Å, $R/R_w = 3.8/4.0\%$ for 52 variables and 703 independent reflections). The compound contains separate close-packed layers of Tl_9Au_2 and Tl_{11} clusters, each with D_{3h} point symmetry, together with isolated Au atoms and 18 K atoms that sheath and separate the units. The gold-containing cluster can be derived directly from the pentacapped trigonal prismatic Tl_{11} through substitution on the two apical (axial) positions followed by a substantial axial compression to generate an Au−Au bond, $d = 2.963$ Å, this action causing the antisymmetric equivalent MO a_2'' to become strongly antibonding and empty. The Tl_9 portion of the cluster is otherwise slightly perturbed. EHMO calculations indicate closed shell configurations for $Tl_9Au_2^{9-}$ and, as before, Tl_{11}^{7-}, leading to formulation of the compound as $(K^+)_{18}(Tl_9Au_2^{9-})(Tl_{11}^{7-})(Au^-)e^-$. The phase is appropriately a metallic conductor ($\varrho_{290} \sim 43$ $\mu\Omega$·cm) and Pauli-paramagnetic, although some localization below 100 K is suggested by its Curie−Weiss behavior.

Introduction

Alkali metal−thallium systems are one of the "gold mines" in cluster chemistry. Besides condensed cluster structures,[2] varieties of isolated cluster units have been discovered and characterized, namely the tetrahedral Tl_4^{8-} in Na_2Tl,[3] trigonal bipyramidal Tl_5^{7-} and defect centered icosahedral Tl_9^{9-} in $Na_2K_{21}Tl_{19}$,[4] compressed octahedral Tl_6^{6-} in KTl[5] and CsTl,[6] pentacapped trigonal prismatic Tl_{11}^{7-} in A_8Tl_{11} (A = K, Rb, Cs)[7,8] and $A_{15}Tl_{27}$ (A = Rb, Cs),[6] and finally, centered icosahedral Tl_{13}^{10-} in $Na_4Rb_6Tl_{13}$ and Tl_{13}^{11-} in $Na_3K_8Tl_{13}$.[9] The rich cluster chemistry appears to pertain to an approximate 1:1 cluster charge:atom ratio and a strong relativistic effect for elemental thallium[9,10] by which the Tl^- state (6 $p_{1/2}$) is additionally favored. Sizes of constituent atoms evidently play a crucial role in establishing what cluster structures are isolated in solid compounds. Size tuning can take place in the cations through mixed alkali metals, as in $Na_2K_{21}Tl_{19}$,[4] $Na_4A_6Tl_{13}$ (A = K, Rb, Cs) and $Na_3K_8Tl_{13}$,[9] or within the cluster anion through addition of an appropriate heterometal. In most cases, the added element goes into an interstitial position, as in $K_8Tl_{10}Zn$ and $K_{10}Tl_{10}Z$ (Z = Ni, Pd, Pt),[6] in the same clusters of the congener indium,[11,12] and in the condensed fullerane $Na_{96}In_{97}Z_2$ (Z = Ni, Pd, or Pt).[13] (Substitution has been relatively rare, principally in $K_8In_{10}Hg$.[14]) Some of the structural and electronic features of these centered compounds are quite similar to those of the well-studied interstitially-stabilized cluster halides of early transition metals.[15,16]

In this article, we report a new and remarkable example of tuning in the K_8Tl_{11} "derivative" $K_{18}Tl_{20}Au_3$ in which substitution for two of the skeletal atoms in the Tl_{11}^{7-} parent functions very differently from earlier examples. The Au atoms afford substantial bonding consequences in the unusual heteratomic polyanion $Tl_9Au_2^{9-}$ which coexists with Tl_{11}^{7-} in the same compound. We further rationalize the observed cluster distortions on the basis of geometrical and electronic considerations and also correlate the structures with the observed electrical and magnetic properties. Efforts to tune with Cu or Ag substitution and to further derivatize $K_{18}Tl_{20}Au_3$ itself are also briefly discussed.

Experimental Section

Synthesis. All the syntheses were carried out by the direct reaction of elements on scale of about 250 mg of total reactants. The surfaces of the K chunks (99.9%, Baker) and Tl bars (99.998%, Johnson Matthey) were cleaned with a scalpel before use, while the Au metal employed was reagent-grade material withdrawn from the USDOE precious metal stockpile and fabricated by Johnson Matthey. The reaction techniques in welded Ta tubing are described in detail elsewhere.[4,17] Because both reagents and products are very sensitive to air and moisture, all operations were handled in N_2- or He-filled gloveboxes with H_2O levels less than 0.1 ppm/vol.

The exploratory syntheses started with a composition of $K_8Tl_{10}Au$, which was heated at 650 °C for 3 d, followed by slow cooling (2 °C/h) to room temperature. The reaction afforded the title compound as a major phase with K_8Tl_{11} as the only X-ray detectable byproduct. Groups of well-shaped blocklike black crystals with metallic luster were

[⊗] Abstract published in *Advance ACS Abstracts,* September 1, 1995.
(1) The Ames Laboratory is operated for the U.S. Department of Energy by Iowa State University under Contract No. W-7405-Eng-82. This research was supported by the Office of the Basic Energy Sciences, Materials Sciences Division, DOE.
(2) Zintl, E.; Dullenkopf, W. *Z. Phys. Chem.* **1932**, *B16*, 195.
(3) Hansen, D. A.; Smith, J. F. *Acta Crystallogr.* **1967**, *22*, 836.
(4) Dong, Z.-C.; Corbett, J. D. *J. Am. Chem. Soc.* **1994**, *116*, 3429.
(5) Dong, Z.-C.; Corbett, J. D. *J. Am. Chem. Soc.* **1993**, *115*, 11299.
(6) Dong, Z.-C.; Corbett, J. D. Unpublished research.
(7) Dong, Z.-C.; Corbett, J. D. *J. Cluster Sci.* **1995**, *6*, 187.
(8) Cordier, G.; V. Müller, V. *Z. Kristallogr.* **1992**, *198*, 281.
(9) Dong, Z.-C.; Corbett, J. D. *J. Am. Chem. Soc.* **1995**, *117*, 6447.
(10) (a) Pyykkö, P.; Desclaux, J. P. *Acc. Chem. Res.* **1979**, *12*, 276. (b) Chen, E. C. M.; Wentworth, W. E. *J. Chem. Educ.* **1975**, *52*, 486.
(11) Sevov, S. C.; Corbett, J. D. *J. Am. Chem. Soc.* **1993**, *115*, 9089
(12) Sevov, S. C.; Corbett, J. D. *Inorg. Chem.* **1993**, *32*, 1059.
(13) Sevov, S. C.; Corbett, J. D. *Science* **1993**, *262*, 880.
(14) Sevov, S. C. Corbett, J. D.; Ostenson, J. E. *J. Alloys Compd.* **1993**, *202*, 289.
(15) Ziebarth, R. P.; Corbett, J. D. *Acc. Chem. Res.* **1989**, *22*, 256.
(16) Corbett, J. D. In *Modern Perspectives in Inorganic Crystal Chemistry;* Parthé, E., ED.; NATO ASI Series C; Kluwer Academic Publishers: Dordrecht, The Netherlands, 1992; p 27.
(17) Sevov, S. C.; Corbett, J. D. *Inorg. Chem.* **1992**, *31*, 1895.

0020-1669/95/1334-5042$09.00/0

Table 1. Selected Data Collection and Refinement Parameters for $K_{18}Tl_{20}Au_3$

fw	5382.3
space group, Z	$P\bar{6}m2$ (No.187), 1
lattice params,[a] Å	
a	10.880(1)
c	14.552(2)
density, g/cm^3	5.990
indep obsd reflns ($I \geq 3\sigma(I)$), variables	703; 52
μ, cm^{-1} (Mo Kα)	629.1
transm coeff range	0.773−1.136
R; R_w[b]	0.038; 0.040

[a] Guinier data, λ = 1.540 562 Å, 23 °C. [b] $R = \sum||F_o| - |F_c||/\sum|F_o|$; $R_w = [\sum w(|F_o| - |F_c|)^2/\sum w(F_o)^2]^{1/2}$; $w = 1/\sigma^2$.

picked out for subsequent single crystal diffraction studies. Once the composition had been established by single crystal X-ray crystallography, stoichiometric proportions that were equilibrated at 500 °C for 1 week, slowly cooled to 350 °C, quenched in ice water, and finally annealed at 250 °C for 1 month gave a well-crystallized single-phase sample of $K_{18}Tl_{20}Au_3$ according to the Guinier powder pattern. X-ray powder patterns for small ground samples mounted between pieces of cellophane were obtained with the aid of an Enraf-Nonius Guinier camera, Cu Kα radiation (λ = 1.540 562 Å), and NIST silicon as an internal standard. The least-squares refinement of 65 lines indexed with the pattern calculated for the structural model gave the lattice constants reported in Table 1. $K_{18}Tl_{20}Au_3$ appears to be a line compound because powder patterns from different compositions give the same cell parameters with deviations less than 0.005 Å (1.4σ). EDAX (energy dispersive analysis by X-ray) studies with a JEOL 840A SEM (and a REBEX DELTA detector) on several crystals confirmed the presence of K, Tl and Au and gave a composition $K_{17.4}Tl_{20}Au_{3.9}$ (± 5%), close to that refined crystallographically. No Rb and Cs analogues have been obtained, although the parent A_8Tl_{11} exist for A = K, Rb, and Cs; neither has $K_{18}Tl_{20}M_3$ been observed for M = Cu or Ag. Size factors, packing requirements for alkali metal cations and substituting anions, and the stability of alternate phases evidently play a significant role here.

Property Measurements. The electrical resistivities of the phase were measured by the electrodeless "Q" method[18] for a sample of 94 mg that had been sieved to a 250−425 μm powder and diluted with Al_2O_3. The "Q" method is based on the change of the quality factor "Q" of an LC circuit caused by rf skin absorption in selectively sized grains when the sample is placed in the cavity of a coil. Measurements were made at 34 MHz over 100−290 K. Magnetic susceptibility data were obtained from a 25 mg sample at fields of 0.1, 1, 3, and 5 T over the 6−300 K with the aid of a Quantum Design MPMS SQUID magnetometer. The sample was held between two fused silica rods which were in turn fixed inside a silica tubing that was sealed at both ends under He. The raw data were corrected for the susceptibilities of the container and the diamagnetism of the atomic cores[19] as well as for the Larmor precession contribution of the delocalized valence electrons in the cluster orbitals.[4,17] The same sample was used for ESR experiments, which were recorded with a Bruker ER-200D spectrometer (X-band, 9.5 GHz) at 295 K.

Structure Determination. Laue and oscillation photographs were used to check the singularity of crystals and to gain information about cell dimensions and symmetry. A block-like crystal ca. 0.25 × 0.25 × 0.21 mm sealed in a thin-wall capillary was mounted on a CAD4 single crystal diffractometer equipped with graphite-monochromated Mo Kα radiation. The 25 reflections from a random search over 14 ≤ 2θ ≤ 30° yielded a hexagonal cell after programmed indexing. Two octants of data were collected and then corrected for Lorentz and polarization effects as well as for strong absorption (μ = 629 cm^{-1}) with the aid of the average of five ψ-scans at different θ values. Intensity data showed no systematic absences, and the intensity statistics suggested an acentric space group, so the model search was started in $P3$. All the thallium and gold atoms were located by the direct method via SHELXS,[20] and the cations were positioned after subsequent least-squares refinements and difference Fourier syntheses. The resultant formula was $K_{18}Tl_{20}Au_3$. Although the structure could be "solved" and refined in $P3$ to R/R_w = 0.63/0.60, some potassium atoms gave nonpositive thermal parameters when refined anisotropically, and there were numerous correlations between variables. More important, inspection of the cell contents indicated mirror symmetry perpendicular to the c axis through the waist of the clusters, which makes the crystal symmetry hexagonal. This and the perpendicular 3-fold axis meant $\bar{6}$ symmetry (note that no 6-fold axis exists!), and additional mirror planes perpendicular to [100], [010], and [$\bar{1}$ $\bar{1}$ 0] made the only possible space group $P\bar{6}m2$. Therefore the structure was re-solved in this space group. All the thallium atoms and the skeletal gold atom were easily assigned following SHELXS according to the environments of the peaks and peak heights. The isolated gold atom and the potassium atoms were assigned after several refinements cycles followed by difference Fourier syntheses. A DIFABS empirical absorption correction was applied, as recommended,[21] after the isotropic refinement with a ψ-scan correction had converged. The final anisotropic refinement, including a second extinction correction, converged at R/R_w = 0.045/0.051, GOF = 1.30. Since the structure is acentric, the enantiomorphic model was checked. This gave clearly better refinement results, R/R_w = 0.038/0.040, GOF = 1.02, and smaller standard deviations for positional and thermal parameters. The R_{int} averaging was 6.6% for observed reflections ($I > 3\sigma(I)$) and 11.2% for all reflections ($I > 0$). The highest residual peak in the final difference Fourier map was 3.30 e$^-$/Å^3, 2.31 Å from Tl2 and 2.41 Å from Tl1 as the top of a rough background. These factors are closely related to an insufficient absorption correction. All calculations were performed using the TEXSAN package.[22] Selected details of the data collection and refinement are listed in Table 1, and positional data and isotropic thermal parameters, in Table 2. Bond distances are given in Table 3. Additional details and the anisotropic displacement parameters are in the Supporting Information; these and the F_o/F_c data are also available from J.D.C.

Table 2. Positional Coordinates[a] and Equivalent Thermal Parameters for $K_{18}Tl_{20}Au_3$

atom	x	z	B_{eq},[b] Å^2
Tl1	0.1812(1)	0.8889(2)	1.60(3)
Tl2	0.4729(1)	0	1.16(3)
Tl3	0.5518(2)	1/2	1.40(4)
Tl4	0.8222(1)	0.6137(2)	1.48(3)
Tl5	2/3	0.6819(3)	1.1(1)
Au1	1/3	0.8982(2)	0.95(9)
Au2[c]	1/3	0.5254(8)	5.0(5)
K1	0	0	2(1)
K2	0.8006(6)	0.8641(9)	2.3(2)
K3	0.160(1)	1/2	3.8(5)
K4	0.4607(6)	0.7144(9)	2.5(2)
K5	0	0.723(2)	2.7(7)

[a] $y = -x$ for all atoms. [b] $B_{eq} = (8\pi^2/3)\sum_i\sum_j U_{ij}a_i^*a_j^*\vec{a}_i\vec{a}_j$. [c] This position refined to be 50(1)% occupied.

One problem with this structure is the disordered Au2 at 1/3, 2/3, ~0.525, which position is split by a mirror plane through the special 1d position ($\bar{6}m2$; 1/3, 2/3, 1/2) perpendicular to the c-axis. This naturally gives rise to a very short Au2−Au2 separation of 0.74(2) Å (50% each). Only in this aspect is the existence of the mirror symmetry perpendicular to the c-axis in question. A lower symmetry model in $P\bar{6}$ still gave the same result. When the mirror symmetry was removed, the symmetry of the model was reduced to trigonal $P3$, but structure solution again indicated two separate Au positions with the same small separation. All these factors suggest an intrinsic disordered feature of the structure. The larger displacement parameters for Au2 and the abnormal U_{33}/U_{11} ratio (3.75:1) for the three neighboring K3 atoms at z = 0.50 further suggest a cooperative effect and real disordering. A model with Au2 located both at 1d ($\bar{6}m2$; 1/3, 2/3, 1/2) and 2h ($3m$; 1/3,

(18) (a) Shinar, J.; Dehner, B.; Beaudry, B. J.; Peterson, D. T. *Phys. Rev.* **1988**, *37B*, 2066. (b) El-Hanany, U. *Rev. Sci. Instrum.* **1973**, *44*, 1067
(19) Selwood, P. W. *Magnetochemistry*; Interscience Publishers: New York, 2nd ed., 1956; p 70.
(20) Sheldrick, G. M. SHELXS-86. Universität Göttingen, Germany, 1986.
(21) Walker, N.; Stuart, D. *Acta Crystallogr.* **1986**, *A39*, 158.
(22) TEXSAN, version 6.0 package, Molecular Structure Corp., The Woodlands; Texas, 1990.

Table 3. Bond Distances in $K_{18}Tl_{20}Au_3$ (<4.5 Å)

Tl1			**Au1**			**K4**		
Tl1		3.234(5)	Tl1	3×	2.870(2)	Tl1	2×	3.681(9)
Tl2	2×	3.196(2)	Tl2	3×	3.019(3)	Tl2		4.16(1)
Au1		2.870(2)	Au1		2.963(7)	Tl3		3.56(1)
K1		3.778(2)	K4	3×	3.59(1)	Tl4	2×	3.798(8)
K2	2×	3.617(6)	**Au2**			Tl5		3.91(1)
K4	2×	3.681(9)	Tl3	3×	4.134(3)	Au1		3.59(1)
K5		4.18(1)	K3	3×	3.29(2)	Au2		3.65(2)
Tl2			K4	3×	3.65(2)	Au2		4.24(2)
Tl1	4×	3.196(2)	K4	3×	4.24(2)	K2	2×	4.05(1)
Au1	2×	3.019(3)	**K1**			K3	2×	4.28(1)
K2	4×	3.794(7)	Tl1	6×	3.778(2)	K4	2×	4.16(1)
K4	2×	4.16(1)	K2	6×	4.25(1)	**K5**		
Tl3			K5	2×	4.04(2)	Tl1	3×	4.18(1)
Tl3	2×	3.749(5)	**K2**			Tl4	3×	3.71(1)
Tl4	4×	3.110(2)	Tl1	2×	3.617(6)	K1		4.04(2)
Tl5	2×	3.419(3)	Tl2	2×	3.794(7)	K2	3×	4.28(2)
K3	2×	3.767(6)	Tl4		3.67(1)	K3	3×	4.42(2)
K4	2×	3.56(1)	Tl5		3.66(1)			
Tl4			K1		4.25(1)			
Tl3	2×	3.110(2)	K2	2×	4.37(2)			
Tl4		3.310(5)	K2		3.96(3)			
Tl5		3.094(2)	K4	2×	4.05(1)			
Tl5			**K3**					
Tl3	3×	3.419(3)	Tl3	2×	3.767(6)			
Tl4	3×	3.094(2)	Tl4	4×	3.597(7)			
K2	3×	3.66(1)	Au2		3.29(2)			
K4	3×	3.91(1)	K4	4×	4.28(1)			
			K5	2×	4.42(2)			

$^2/_3$, z) was also tested, but refinements yielded no occupancy for the former, as before. The refined occupancy in 2*h* was 50 (1)% for Au with a well-defined U_{33}/U_{11} ratio of 1.13; hence this position was fixed at half-occupancy in the final model. (Isotropic treatment of Au2 gave the very same positional B and residual parameters.) A full occupancy model for all other atoms was supported by alternate refinements of the multiplicities of one type of atom while the others were so, all of which showed deviations from unity of less than 3σ. Therefore all were so fixed in the final refinement.

Since Tl and Au are crystallographically indistinguishable, one reason for assigning the disordered position to Au, and not Tl, was based on the consideration of electron counts in the overall structure (below). Au^- is well-known, while there is no precedent for an isolated Tl^-. Finally, although disorder complicates the assessment, the average K−Au2 distance here, 3.47 Å, is much closer to typical bond distances for K−Au (~3.45 Å) vs K−Tl (~3.75 Å). The K−Au value is the average from K_2Au_3 (3.48 Å), KAu_2 (3.37 Å), and KAu_5 (3.50 Å), where the overall range is 3.2−3.7 Å.[23] Comparatively, the two skeletal Au1 positions are easily distinguished in terms of the apparent geometrical distortion from the parent Tl_{11}^{7-} as well as their shorter distances to the neighboring atoms (2.94 Å average) in comparison with Tl−Tl separations. (The Au−Tl distance in $AuTl_2$ is 3.07 Å.[24]) Evidence for the assigned quantity of gold came from EDAX results which not only confirmed the presence of Au, but also gave a composition close to $K_{18}Tl_{20}Au_3$. Further support, and the most convincing, for the assigned composition came from a synthesis reaction with that stoichiometry which gave a single phase by Guinier powder diffraction (≥97% yield). Of course, no analogues of this geometry or crystal symmetry are observed in the pure binary K−Tl system either.

Results and Discussions

Cluster Skeletons. The most remarkable features of this structure are, first, the presence of an isolated "naked" heteroatomic polyanion $Tl_9Au_2^{9-}$, and second, the coexistence with the "parent" pentacapped trigonal prismatic Tl_{11}^{7-}, the same

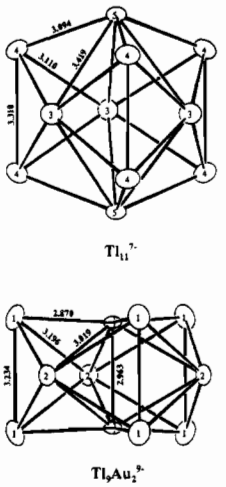

Figure 1. Isolated clusters (D_{3h}) in $K_{18}Tl_{20}Au_3$: top, Tl_{11}^{7-}; bottom, $Tl_9Au_2^{9-}$. The open ellipsoids stand for Tl and crossed ellipsoids, for Au. The principal 3-fold axis lies vertical through Tl5 and Au1 (90% thermal displacement ellipsoids).

skeleton found before in A_8Tl_{11} (A = K, Rb or Cs).[7,8] Both are shown in Figure 1. (Charges assigned to clusters are based on the EHMO calculations and the observed properties, below.) The coexistence of two separate thallium cluster anions is not new, but rather was reported previously in $Na_2K_{21}Tl_{19}$ where Tl_5^{7-} and Tl_9^{9-} units order in layers.[4] These unusual compounds illustrate how delicately electronic and packing requirements can combine to create unprecedented three-dimensional structures in which isolated cluster anions are trapped. Since the cluster skeleton of $Tl_9Au_2^{9-}$ can be viewed as a modified Tl_{11}^{7-} with two apical capping Tl atoms replaced by interbonded Au atoms (Figure 1), the compound is, in this sense, a derivative of the parent K_8Tl_{11}. The crystal symmetry is actually higher than that of K_8Tl_{11}, i.e., $P\bar{6}m2$ (hexagonal) versus $R\bar{3}c$ (rhombohedral), and a D_{3h} point symmetry for both clusters in $K_{18}Tl_{20}Au_3$ vs D_3 for Tl_{11}^{7-} in K_8Tl_{11}. The higher symmetry imposes more constraints on the interatomic connections, making all T13−T14 distances equivalent and yielding the four types shown in Figure 1, instead of the five in K_8Tl_{11}.[7,8] The principal geometric characteristic of Tl_{11}^{7-} [7] (and In_{11}^{7-} [25,26]) is a pronounced compression of the "ideal" model along the 3-fold axis to generate six new contacts between end-capping and waist-capping atoms (T15−T13) at the expense of six bonds (edges) on the two basal triangles of the prism. The overall differences between the Tl_{11}^{7-} units in K_8Tl_{11} and $K_{18}Tl_{20}Au_3$ are extremely small with only a small further axial compression (T15−T15) from 5.33 to 5.29 Å, an increase in the prism height (T14−T14) from 3.22 to 3.31 Å, and an accompanying axial-to-prism (T14−T15) decrease from 3.15 to 3.09 Å. The different Tl−Tl separations range from 3.094(3) to 3.419(5) Å with an average 3.253(3) Å over the Tl_{11} polyhedron, the same as 3.256(3) Å in K_8Tl_{11}. These small changes are presumably all related to packing effects.

What strikes one most is the geometry of the $Tl_9Au_2^{9-}$ unit. The distortion from Tl_{11}^{7-} is manifest, though the cluster topology looks very similar. Actually, the Au−Au bond is the only significant change in the connections. The figure has been greatly (and further) squashed along the 3-fold axis so that the two gold atoms now lie 0.14 Å inside the basal faces of the trigonal prism faces defined by Tl1, presenting a slightly *concave* polyhedron. A nonconvex feature is very uncommon

(23) KAu_2: Range, K.-J.; Rau, F.; Klemment, U. *Acta Crystallogr.* **1988**, *44C*, 1485; K_2Au_3: Krieger-Beck, P.; Brodbeck, A.; Strähle, J. *Z. Naturforsch.* **1989**, *44B*, 237; KAu_5: Raub, C. J.; Compton, V. B. *Z. Anorg. Allg. Chem.* **1964**, *332*, 5.

(24) Havinga, E. E., Damsma, H.; Hokkeling, P. *J. Less-Common Met.* **1972**, *27*, 169.

(25) Sevov, S. C.; Corbett, J. D. *Inorg. Chem.* **1991**, *30*, 4875.

(26) Blase, W.; Cordier, G.; Müller, V.; Häussermann. U.; Nesper, R.; Somer, M. *Z. Naturforsch.* **1993**, *48B*, 754.

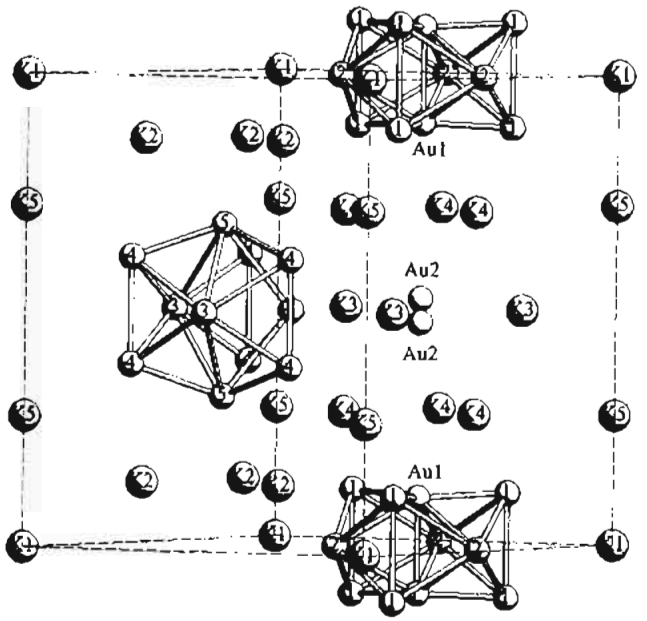

Figure 2. Distribution of the two cluster units, the isolated Au2 atom, and the "solvating" cations as well as the double potassium layer in a unit cell. The *c* axis lies vertical.

for stable polyhedral clusters and clearly must result from the strong transannular bond formed between the two end-capping Au atoms. The Au−Au bond, 2.963(7) Å (PBO = 0.63 taking 1.34 Å for the Pauling single bond radius[27]) falls in the range 3.00 ± 0.25 Å found in many polygold(I) cluster complexes,[28,29] but it is significantly longer than those in intermetallics formally containing partially reduced gold, e.g., in A_2Au_3 (A = K, Rb) where the extreme Au−Au distances are 2.69 and 2.83 Å.[30] The observed configuration is evidently a compromise among the polyhedral convexity, the Au−Au bonding, and the p−π bonding within the two Tl1 triangles that is discussed below. The Tl−Au distances are notably shorter than their counterparts in Tl_{11}^{7-}. Indeed, the Tl1−Au1 distance of 2.870(2) Å (PBO = 0.86 assuming a 1.44 Å Tl−Tl single bond radius and additivity) is indicative of strong bonding interactions within this (near) plane. Correspondingly, the edges of this triangle shrink from 5.08 Å in Tl_{11}^{7-} to 4.97 Å in $Tl_9Au_2^{9-}$ and the height of the trigonal prism also decreases by 0.08 Å, in parallel with the added Au−Au bonding. The separation between waist-capping Tl2 atoms is correspondingly, and markedly, increased from 3.75 to 4.56 Å, presumably because otherwise close contacts with the Au atoms would weaken the preferred p−π bonding in the basal planes. (The total bonding capacities for an atom are often almost constant.) Such an arrangement leaves Tl2−Au1 = 3.019 Å and Tl2−Tl1 = 3.196 Å, about 0.09 Å longer than in Tl_{11}^{7-}. The result is clearly different from the only other observed nine-atom cluster Tl_9^{9-} (C_{2v}) in $Na_2K_{21}Tl_{19}$, which is a defect centered icosahedron with four adjacent vertices missing.

Cation Distributions and Cluster Packing. Figure 2 shows the space partitioning among cluster units, isolated Au atoms, and the "solvating" cations in the unit cell. The 3-fold axial symmetry along $\bar{c}$ through Tl_{11}^{7-} and $Tl_9Au_2^{9-}$ places these units in separate layers that alternate in a pseudo-*hcp* pattern. Figure 3 is a [001] projection of this with shaded pentacapped trigonal prisms for Tl_{11}^{7-} (centered at $z = {}^1/_2$) and shaded tricapped trigonal prisms for $Tl_9Au_2^{9-}$ (centered at $z = 0$; the two Au atoms are inside the polyhedron and not seen). The neighboring cluster layers are, analogous to K_8Tl_{11}, separated by a double potassium layer composed of K2, K4, and K5 atoms. The shortest distance between alkali-metal atoms is the 3.96(3) Å K2−K2 separation. The closest intercluster Tl−Tl separations is 5.242(2) Å and occurs between prismatic vertex atoms in the adjacent layers, i.e., Tl1 and Tl4.

The substantial "solvation" of polyanions by alkali metal cations is evident in Figures 2 and 3 and appears to establish a harmonious "ionic packing" pattern. The specific roles of the cations about the cluster faces, edges, and vertices are to compensate anionic charge and to bridge between clusters, often in dual bridging functions. As in K_8Tl_{11},[7] each Tl_{11} unit is surrounded by 24 K atoms. Six waist Tl3−Tl4−Tl4 triangles are each capped by a K3 atom that is in turn shared by another waist triangle of the neighboring cluster in the same layer, while each end of Tl_{11} is capped, bridged, and exo-bonded by K4 (μ_4 to Tl3−Tl4−Tl4−Tl5), K2 (μ_2 to Tl4−Tl5), and K5 (to Tl4), respectively, three of each type. On the other hand, each Tl_9Au_2 unit is sheathed by 27 K atoms with the basal faces similarly capped by K4 (μ_4 to Tl1−Tl1−Tl2−Au1) and exo-bonded by K5 (to Tl1) atoms. The differences in cation arrangements about the two clusters is shown in the different bridging roles of K1 and K2 atoms. The former bridges each prismatic edge instead of lying on a waist triangle, and this atom is also shared by two other prismatic edges on neighboring clusters in the same layer. And the K2 atom is no longer bridged intercluster to Tl4−Tl5 edges but to the waist-to-vertex (Tl1−Tl2) edge in $Tl_9Au_2^{9-}$. The cation environments around the two clusters are illustrated in the Supporting Information. All of the thallium atoms are in a more or less distorted icosahedral environments if distant triangular faces at ~5 Å are included. And all atoms lie on σ_v planes, with Tl2, Tl3, K1, and K3 in the σ_h plane through the clusters as well.

Another aspect of the structure worth mentioning is the presence of an isolated Au2 atom in a tricapped trigonal prismatic cavity defined by cations (3K3 + 6K4; drawing in Supporting Information). The position is not exactly on the σ_h plane (Figure 2) but slightly shifted along the *c* axis, yielding a pair of half-occupied disordered sites with nearly coplanar neighbors Au2−K3 = 3.29(2) Å (×3) plus Au2−K4 = 3.65(2) Å (×3) in the closest layer along $\bar{c}$ and, in the other direction, Au2−K4 = 4.24(2) Å (×3). The reason for the split position obviously derives from the elongated environment provided. A model with ordered Au2 on the midpoint (1*d*) would produce six long Au2−K4 distances of 3.94 Å, much longer than typical 3.5 Å distances in K−Au intermetallic compounds[23] and too great to effectively bind the Au2 anion. The elongated ellipsoid for the K3 atoms about the waist of this site ($U_{33}/U_{11} = 3.75$) is clearly related to the splitting. The next coordination sphere around Au2 consists of two Au1 (5.43 Å) and three Tl3 (4.13 Å) in a trigonal bipyramidal arrangement. On the basis of the packing and the electronic configuration of Au, we suppose a formal −1 charge for the isolated Au2 ($5d^{10}6s^2$). The semiconducting CsAu[31] provides an obvious analog.

Finally, following the above assignments and the bonding discussion below, the compound is formulated as $(K^+)_{18}(Tl_{11}^{7-})(Tl_9Au_2^{9-})(Au^-)e^-$, the last species originating with the odd number of valence electrons in $K_{18}Tl_{20}Au_3$ (18 × 1 +

(27) Pauling, L. *The Nature of the Chemical Bond*, 3th ed.; Cornell University Press: Ithaca, NY, 1960; p 400.
(28) Vicente, J.; Chicote, M.-T.; Lagunas, M.-C. *Inorg. Chem.* **1993**, *32*, 3748.
(29) Schmidbaur, H. *Gold Bull.* **1991**, *23*, 11. Zeller, E.; Beruda, H.; Schmidbaur, H. *Inorg. Chem.* **1993**, *32*, 3203.
(30) Zachwieja, U. *J. Alloys Compd.* **1994**, *206*, 277 and references therein.
(31) Overhof, H.; Fischer, R.; Vulli, M.; Hensel, F. *Ber. Bunsen-Ges. Phys. Chem.* **1976**, *80*, 871.

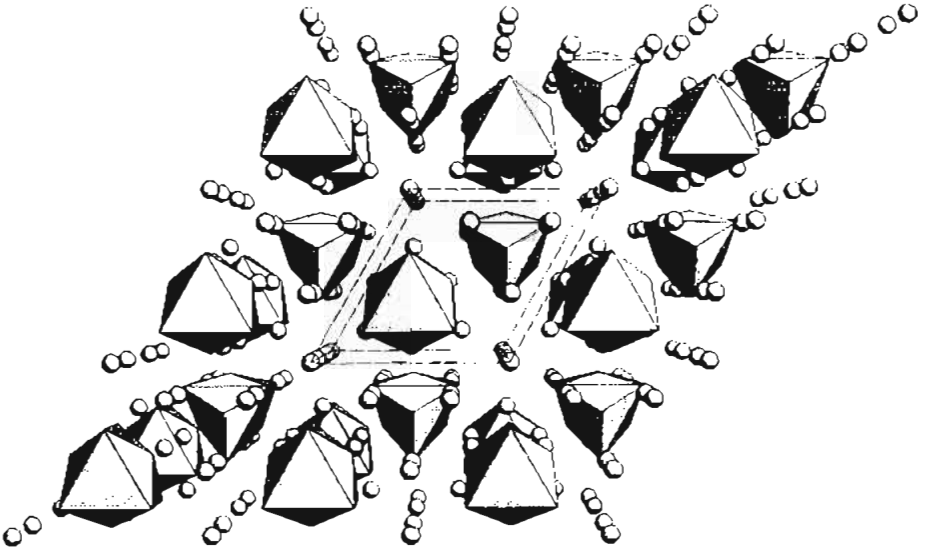

Figure 3. [001] projection of cluster units, showing the pseudo-*hcp* stacking along the *c* axis. The shaded tricapped trigonal prisms represent $Tl_9Au_2^{9-}$ with its center at $z = 0$, and the shaded pentacapped trigonal prisms, Tl_{11}^{7-} with its center at $z = 1/2$.

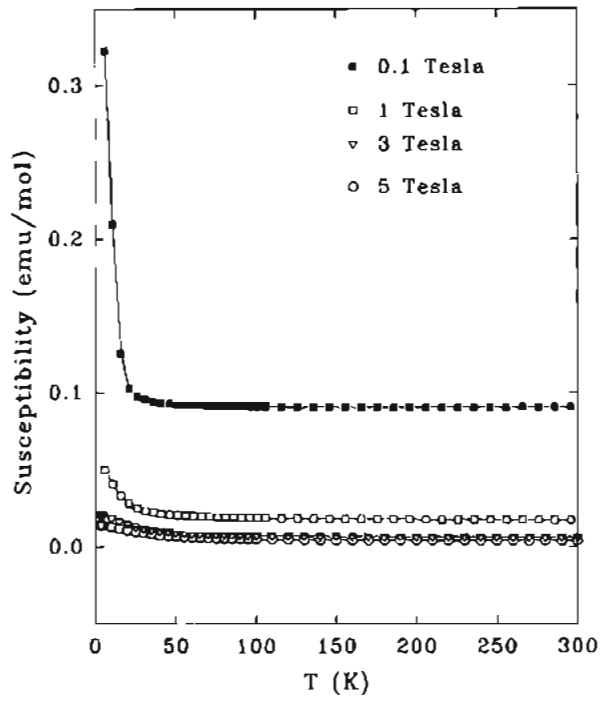

Figure 4. Molar susceptibilities of $K_{18}Tl_{20}Au_3$ at 0.1, 1, 3, and 5 T.

$20 \times 3 + 3 \times 1$). The result is very similar to the formulation of metallic $(K^+)_8(Tl_{11}^{7-})e^{-7}$ and $(K^+)_8In_{11}^{7-}e^{-25}$ where cation packing and anion "solvation" dominate, the same factors that leave a "hole" in the anion MOs in $Na_4A_6Tl_{13}$, A = K, Rb, and Cs.[9]

Properties and Bonding. Magnetic susceptibility data for $K_{18}Tl_{20}Au_3$ at four different fields are shown in Figure 4. The most obvious characteristic is the substantially temperature-independent susceptibility above ~50−100 K, a Pauli-paramagnetic-like property of $\sim 6(2) \times 10^{-3}$ emu/mol (or $7(2) \times 10^{-6}$ emu/cm^3) at 3 T. (Diamagnetic corrections were applied to exclude the contributions from the cores[19] (-10.34×10^{-4} emu/mol) and the Larmor precession[32] (-5.59×10^{-4} emu/mol) of the skeletal electrons in each cluster.) The field dependence of susceptibility for this kind of material, as usually observed, is qualitatively explained in the following. The magnetization M for Pauli-paramagnetic materials is proportional to $[(\epsilon_F + \mu H)^{3/2} - (\epsilon_F - \mu H)^{3/2}]$ where ϵ_F is the Fermi energy, μ the intrinsic magnetic moment of the particle, and H the applied field.[33] Since μH is only of order of 10^{-4} ϵ_F even at 10^4 G, the susceptibility defined by M/H can be approximately expressed as

$$\chi = \chi_{Pauli} - cH^2 + \ldots$$

in which $\chi_{Pauli} = 3N\mu^2/2\epsilon_F$ and c is a parameter related to the basic properties of the particle, but much smaller than χ_{Pauli} ($\sim 10^{-8}$). Hence, though the magnetization increases with increasing field, the susceptibility variation shows an opposite trend, i.e., decreasing with the increase of an applied field. Below ~100 K, normal paramagnetism begins to dominate. A nonlinear fitting of this region for 3T with the function $\chi_M = C/(T - \Theta) + \chi_0$ gives a Curie−Weiss behavior with an effective magneton number of ~1.8 μ_B per formula unit and a Weiss constant of ~−20 K (χ_0 is the background susceptibility or TIP). The rapid increase of susceptibility in the very low temperature (<8 K at 3 T) region, the so-called "Curie tail", appears related to a presumed antiferromagnetic interaction (or impurity).

ESR data at 295 K show a broad peak around ~3360 G, indicating a single type of spin with $g \sim 2.01$. The spectrum is shown in the Supporting Information. The hyperfine structure, two small side bands about a strong central peak, is not yet understood, but it is supposedly simplified owing to poor resolution, with weak couplings probably immersed in the central peak. Data collected at 100 K presented a slightly sharpened peak, but the general picture remained the same.

Temperature-dependence resistivity data for $K_{18}Tl_{20}Au_3$ are shown in Figure 5 and indicate a metallic behavior with $\partial\rho/\rho\partial T = +0.33(1)\%$ K^{-1}, and $\rho_{290} \sim 43$ $\mu\Omega$·cm. (As a comparison, Al has $\rho_{298} = 2.65$ $\mu\Omega$·cm.) This result together with the magnetic data and the structure suggest that, first, there is one unpaired electron per cell, and, second, this electron is probably not well localized either on the clusters or the isolated Au atom, but it is more or less delocalized in the lattice, possibly in the double K layers. Because of the small concentration of unpaired electrons, spin-spin interactions between these are

(32) Ashcroft, N. W.; Mermin, D. N. *Solid State Physics*; Holt, Rinehart and Winston: Philadelphia, 1976; p 649.

(33) Pathria, R. K. *Statistical Mechanics*, Pergamon Press: New York, 1972; pp 222−226.

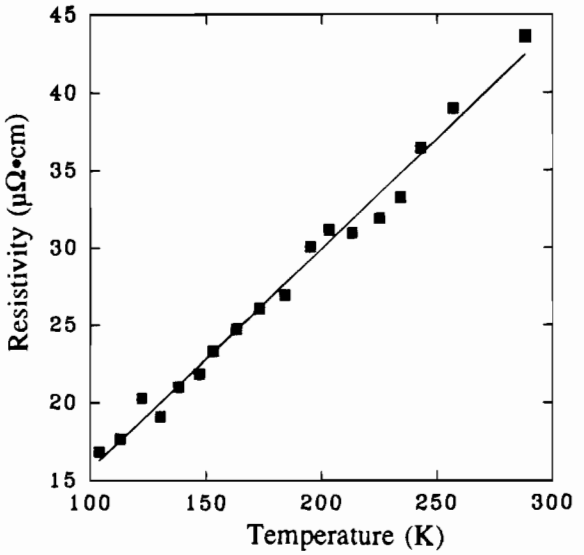

Figure 5. Temperature dependence of the resistivity of $K_{18}Tl_{20}Au_3$ over 100−290 K by the "Q" method.

negligible, so the ESR line broadening is probably related to the interaction of weakly localized unpaired electrons with thermal vibrations of the lattice (spin−lattice relaxation). This results in frequent electron transitions, short relaxation times and broad peaks, but the relaxation time is not so short as to wipe out the ESR signal. In other words, the unpaired electrons are far away from a free electron approximation. With decreasing temperature, the unpaired electrons tend to be more trapped in the structure, ESR signals are slightly sharpened and susceptibilities increase slightly. It would be useful to extend the ESR and conductivity measurements into the Curie−Weiss region.

Bonding. In order to understand the electron count, the geometric distortion of the cluster on thallium substitution, and the observed properties, electronic structure calculations were carried out on the isolated Tl_{11} and Tl_9Au_2 clusters by EHMO methods.[34] The validity of the EHMO method in such a system and the justification of the atomic parameters used for Tl were described in previous papers,[5,9] while the parameters for Au were taken from Komiya and co-workers.[35] Relativistic effects[36] for Tl and Au will definitely change individual energy levels because of the spin−orbit splitting of $6p_{1/2}$ and $6p_{3/2}$ (~0.95 eV[37] in Tl(g)). But, as concluded before,[9] the general bonding picture still remains basically the same as found from a routine EHMO calculation because of mixing of the p levels. Thus relativistic effects are not our concern for the present, although these are probably responsible for some of the stability of Au^-. The observed Tl_{11}^{7-} and $Tl_9Au_2^{9-}$ geometries (D_{3h}) were used in the calculation with z the principal 3-fold axis, and no charge iteration calculations were done. The influence of distortion following Au substitution are clearly demonstrated in Figure 6. In Tl_{11}^{7-} on the left, only the top two lone-pair orbitals ($1a_1'$ and $1a_2''$) out of the eleven largely 6s-based sets are shown under the 6p-dominated band, with the rest omitted for clarity. In $Tl_9Au_2^{9-}$ on the right, the 10 low-lying Au 5d nonbonding

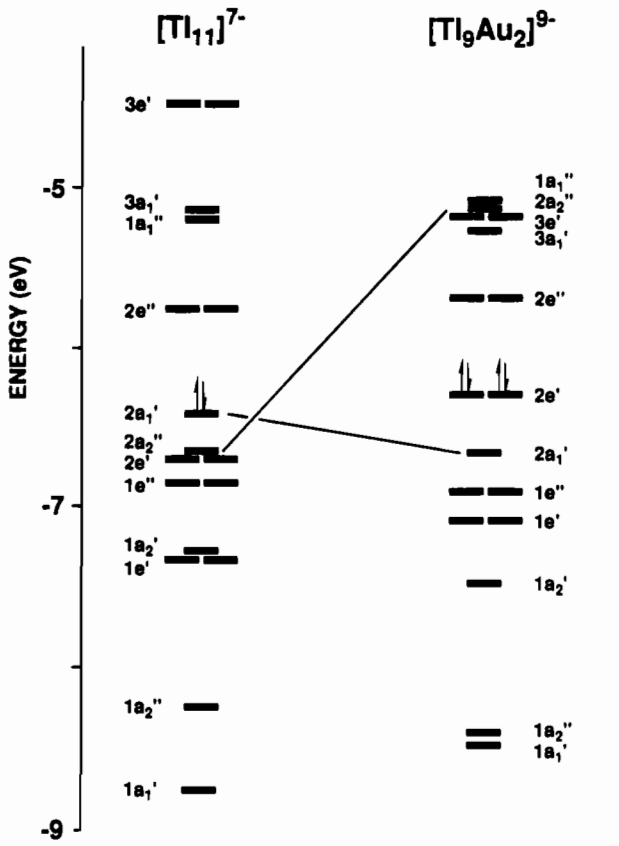

Figure 6. MO diagrams for the observed D_{3h} Tl_{11}^{7-} (left) and $Tl_9Au_2^{9-}$ (right) polyanions.

orbitals and nine Tl 6s lone pairs are also neglected, while the lowest two shown are predominately similar Au s pairs.

The bonding picture of hypoelectronic Tl_{11}^{7-} has been well established for A_8Tl_{11} (A = K, Rb, Cs) and A_8In_{11}.[7,25,26] The axial compression coupled with prism face expansion of a regular (hypothetical) pentacapped trigonal prism remains the first, beautiful example[25] of a means to reduce charge, improve bonding, and reach a stable hypoelectronic anion, as has also been demonstrated by Tl_6^{6-} and $Tl_{10}Zn^{10-}$ and earlier, by some indium analogues.[5,6,11,12] The present calculations likewise show that a Tl_{11}^{7-} polyanion is the optimum electronic configuration with the first 20 valence MOs filled and a HOMO−LUMO gap of ~0.66 eV, while the first 19 (not counting Au 5d) would be filled to give a $Tl_9Au_2^{9-}$ polyanion with a gap of ~0.60 eV. Overlap population analyses in the HOMO levels $2a_1'$ at −6.43 eV (+0.317) and $2e'$ at −6.30 eV (+0.335) in the respective cases indicate these are strongly bonding orbitals, while the LUMO levels $2e''$ in both are almost nonbonding according to the net overlap populations, −0.018 and +0.026. The Tl_{11}^{7-} cluster does not exhibit a geometry like $Tl_9Au_2^{9-}$ simply because that would force electrons into the LUMO $2e''$ and make the bonding situation much more unfavorable unless the charge were decreased to −5. The reason why charge reduction does not occur must have something to do with the number of cations required for adequate "solvation". Although the two clusters have energy-consistent gaps in these simple calculations, addition of at least suitable coulombic energies of "solvation" would be necessary to show that they have something like consistent Fermi energies.

As for $Tl_9Au_2^{9-}$, replacement of the two axial Tl atoms by the electron-poorer Au causes a further, and substantial, compression of the trigonal prism along the 3-fold axis. The bonding interactions (σ and π) between end-capping (axial) atoms and the rest (e.g., in a_1', a_2'', and e') change correspond-

(34) Hoffmann, R. *J. Chem. Phys.* **1963**, *39*, 1397.
(35) Komiya, S.; Albright, T. A.; Hoffmann, R.; Kochi, J. K. *J. Am. Chem. Soc.* **1977**, 99, 8440. The atomic parameters used in the EHMO calculations are as follows. Tl: 6s, $\zeta = 2.14$, $H_{ii} = -11.60$ eV; 6p, $\zeta = 2.04$, $H_{ii} = -5.80$ eV.[5] Au: 6s, $\zeta = 2.60$, $H_{ii} = -10.92$ eV; 6p, $\zeta = 2.58$, $H_{ii} = -5.55$ eV; 5d, $\zeta_1 = 6.16$, $\zeta_2 = 2.79$, $H_{ii} = -15.07$ eV, $c_1 = 0.6441$, $c_2 = 0.5355$.
(36) Pyykkö, P. *Chem. Rev.* **1988**, *88*, 563.
(37) Desclaux, J. P. *At. Data Nucl. Data Tables* **1973**, *12*, 311. Pyykkö, P. *Chem. Rev.* **1988**, *88*, 563.

ingly (Figure 6). The most striking characteristics are seen in the axial $2a_1'$ and $2a_2''$, the skeletal orbitals with significant p_z-orbital contributions on the Au atoms that are in-phase and out-of-phase, respectively. The result is a tricapped trigonal prism squashed along the 3-fold axis to shorten the axial distance from 5.29 Å for Tl_{11}^{7-} (without significant p-orbital interactions) to 2.96 Å in $Tl_9Au_2^{9-}$ (PBO = 0.63, with a p_z-p_z overlap population of +0.18 in $2a_1'$). Why don't the two Au atoms go closer? This must be because these Au atoms not only form a strong Au−Au bond but also play an important role in holding the cluster together. A balance is reached between formation of Au−Au bond and Au bonding with other Tl neighbors, including p−π delocalizations with Tl1 within the two triangular faces of the prism ($2a_1'$). With the Au1−Tl1 distance as short as 2.871(2) Å, a Au1−Tl1 p_z-p_z overlap population of 0.03 (×3) is also achieved with the Au atom only 0.14 Å inside the end triangles. Since the Tl2 atoms do not have a geometrical advantage in forming significant pπ bonding, they instead move outward upon the slight contraction of the basal triangles in order to keep a more nearly normal Tl−Au separation of 3.02 Å (as in $AuTl_2$, 3.07 Å[24]) and also as a consequence of the conservation of the total bonding capacity by the Au1 atoms. The *skeletal* bonding electrons decrease from 18 in Tl_{11}^{7-} to 16 in $Tl_9Au_2^{9-}$, a difference that can be classically rationalized as those unnecessary after the formation of the Au−Au bond, because of the conversion of $2a_2''$ to antibonding. The total cluster electrons (including $6s^2$) likewise decrease from 40 to 38. An alternate expression of the changes is to note that the direct substitution product $Tl_9Au_2^{7-}$ is short four electrons. This is compensated by (a) Au−Au bond formation, which empties what becomes σ^* $2a_2''$, and (b) the addition of two electrons to give $Tl_9Au_2^{9-}$. Gold is effectively reduced in the process and has $6s^2$ pairs in the lower band, with the $5d^{10}$ levels even lower.

The total of 80 electrons in the anions in $K_{18}Tl_{20}Au_3$ comes from 40 in Tl_{11}^{7-}, 38 in $Tl_9Au_2^{9-}$, and 2 for isolated Au^-. The total available valence electrons is 81, so there is one extra and evidently unpaired electron. This electron if delocalized will yield a Pauli paramagnetism, but if localized will produce a Curie−Weiss behavior. The susceptibility measurements demonstrate it belongs to the former case above about 100 K, consistent with the observed metallic property. Similar arguments were previously employed to rationalize the metallic and Pauli-paramagnetic properties of the parent $(K^+_8)(Tl_{11}^{7-})e^-$ and the indium prototype.[7,25] Analogous to the behavior of these well-established polyanions, the unpaired electron is unlikely to be localized on $Tl_9Au_2^{9-}$ because it would occupy a higher-lying nonbonding state, or on the isolated Au atom either because that would put the electron in high-lying 6p orbital on Au^{2-} without any effective bonding compensation. At low temperatures, this odd electron may become trapped in the K sublattice, or even in the LUMO in a cluster unit, either resulting in the possible Curie-Weiss behavior at <100 K. The observed ESR spectra must originate either from an impurity in the sample or, better, from a conduction process that looks metallic in resistivity at 35 MHz but involves a localized electron on a faster observation scale.

The Tl_{11}^{7-} cluster is widely seen and of significant stability. The line phases A_8Tl_{11} are formed over wide composition ranges for A = K, Rb, and Cs. The same isolated cluster is also found in the $A_{15}Tl_{27}$ (A = Rb, Cs) (and in $Rb_{14}CsTl_{27}$) which contain additional layers of Tl_{11} condensed through sharing of the three prismatic edges.[6] The Tl_{11}^{7-} skeleton can be modified by substitution of some of its vertex atoms, as exemplified by this work. However, it is size factors that seem to play the dominant role in the nature of the solid phases formed. No analogues of the present compound were observed for A = Na, Rb, or Cs under the same synthetic conditions, presumably because of poorer packing. Adequate foresight regarding other factors and unprecedented structures is usually impossible to achieve. However, Cu is probably much too small to form a Tl_9Cu_2 cluster, as observed. Although silver would seem to be a good candidate, it forms another unidentified structure type. The Ag−Au difference maybe mainly caused by relativistic effects on the s and the p orbitals of the latter.[36] On the other hand, the isolated Au found in the structure should in principle afford more opportunities for electronic tuning. For example, were this to be replaced by simple dinegative anions of M = Se, Te, or Pt, the $K_{18}Tl_{20}Au_2M$ phase would be electron-precise and diamagnetic. Unfortunately, such simple modifications rarely work out, and preliminary investigations indicate such phases do not form. Likewise, if M were Sn^{-4} or Pb^{-4}, then a diamagnetic salt with $Tl_9Cd_2^{7-}$ or $Tl_9Hg_2^{7-}$ polyanions might be possible. Further research is in progress. A $Tl_{10}Hg^{8-}$ analogue of $In_{10}Hg^{8-}$ [14] does not appear to exist.

In summary, the diversity of known "naked" cluster units of thallium: Tl_4^{8-}, Tl_5^{7-}, Tl_6^{6-}, Tl_9^{9-}, Tl_{11}^{7-}, Tl_{13}^{10-}, and Tl_{13}^{11-} allows size tuning with the cations to be very productive. Likewise, only a single cation type yields the present $K_{18}Tl_{20}Au_3$. Although charges assigned to clusters are based on an unreasonable extreme of complete electron transfer from alkali metal cations to thallium polyanions, the spirit it reflects—the Zintl concept, *electron transfer (ionic part), and formation of closed shell anionic substructures (covalent part)*—represents a practical chemical guideline for designing experiments and understanding structures.[9,38-40] More opportunities are thereby open for one to tune chemistry with the aid of electron counting rules (e.g., Wade's rules[41]) in ternary or higher alkali-metal−thallium systems than in simple binary systems. However, the results of such synthetic explorations are, to a greater degree, governed by the more complex and unanticipated features. And it is this unpredictable character that makes the synthesis of new materials fascinating and challenging. Gold is still where you find it.

Acknowledgment. The authors are indebted to M. Xu and D. K. Finnemore for the magnetic measurements and to D. C. Jiles and R. E. McCarley for discussions about magnetic properties.

Supporting Information Available: Tables of crystallographic details and anisotropic displacement parameters, drawings of the cation distributions about the two clusters and the isolated Au2 atom, and the ESR spectrum (5 pages). This material is contained in many libraries on microfiche, immediately follows this article in the microfilm version of the journal, and can be ordered from the ACS; see any current masthead page for ordering information.

IC950280X

(38) Zintl, E. *Angew. Chem.* **1939**, *52*, 1. Klemm, W.; Busmann, E. *Z. Anorg. Allg. Chem.* **1963**, *319*, 297.
(39) Corbett, J. D. *Chem. Rev.* **1985**, *85*, 383.
(40) Schäfer, H. *Annu. Rev. Mater. Sci.* **1985**, *15*, 1.
(41) Wade, K. *Adv. Inorg. Chem. Radiochem.* **1976**, *18*, 1.